

Efficient Endocytosis of Inorganic Nanoparticles with Zwitterionic Surface Functionalization

Emile Drijvers,^{1,2} Jing Liu,³ Aranit Harizaj,³ Ulrich Wiesner,⁴ Kevin Braeckmans,^{2,3} Zeger Hens,^{1,2} Tangi Aubert^{1,2,4*}

¹ Department of Chemistry, Ghent University, 9000 Ghent, Belgium

² Center for Nano and Biophotonics, Ghent University, 9000 Ghent, Belgium

³ Laboratory of General Biochemistry and Physical Pharmacy, Faculty of Pharmacy, Ghent University, 9000 Ghent, Belgium

⁴ Department of Materials Science and Engineering, Cornell University, Ithaca, NY, 14853, United States

* E-mail: tangi.aubert@ugent.be

Keywords : nanomaterials, SBS, endosomal uptake, bioimaging, NMR

Abstract

PEGylation, which has traditionally been the method of choice to enhance the colloidal stability of nanostructures designed for biological applications, and to prevent non-specific protein adsorption, is now being challenged by short zwitterionic ligands. Inspired by the zwitterionic nature of cell membranes, these ligands have the potential to push forward the field of nanoparticles for nanomedicine. In this work, we report a thorough analysis of the surface chemistry of silica coated luminescent CdSe/CdS quantum dots functionalized with either PEG-silane or zwitterionic sulfobetaine-silane by quantitative nuclear magnetic resonance spectroscopy. We demonstrate the differences in the cellular uptake propensity between particles with these two ligands. While both ligands offer good colloidal stability in crowded cell culture medium, the zwitterionic functionalized nanoparticles with an optimized ligand density showed to be more easily endocytosed by HeLa cells. This approach can readily be transferred to other nanoparticle systems offering a wealth of unique properties, with great potential for intracellular bio-applications.

1. Introduction

Diagnostic and therapy techniques in modern nanomedicine have benefited in the past decades from the growing interest and significant advancement in the development of functional nanoparticles (NPs).¹⁻³ New generation NPs have emerged as important players in the development of high contrast bioimaging and in offering novel diagnostic and therapeutic opportunities. Due to their unique properties (luminescent, magnetic, plasmonic, etc.), and in combination with specific surface functionalization, NPs have become an interesting class of materials for cell labeling, selective targeting of biomolecules, sensitive biosensing, smart drug delivery strategies and other theranostics applications.⁴⁻⁶ To achieve their full potential, NPs developed for biological applications should meet important criteria, including a robust colloidal stability in a variety of complex environments. Indeed, the colloidal stability observed for inorganic NPs in a simple solvent system is often challenged once in dense and crowded biological media. On the other hand, for NPs specifically designed for intracellular applications, an efficient cellular uptake is also required, which is commonly achieved via endocytic pathways.⁵ Several approaches have been

47 developed for the receptor-mediated endocytosis of NPs through their functionalization with
48 targeting ligands such as peptides, aptamers, or antibodies,⁷ but those are often very expensive and
49 each requires a dedicated chemistry.

50 Water-dispersible NPs for biological applications are typically functionalized with
51 polyethylene glycol (PEG) and PEG derivatives,⁸⁻¹¹ which provide excellent colloidal stability
52 while reducing opsonization and nonspecific protein interactions. However, while PEG ligands
53 prevent the formation of a protein corona around the NPs, PEGylated NPs exhibit a reduced
54 cellular uptake in cultured cells, as compared to the bare NP counterparts.¹²⁻¹⁴ To overcome this
55 limitation, zwitterionic ligands are being investigated for their anti-biofouling property, as an
56 alternative to PEGylation.^{15, 16} Indeed, zwitterionic ligands have been reported to also reduce
57 nonspecific protein adsorption,¹⁷⁻²⁰ while providing excellent stability in high salt concentration
58 solutions and in biological media over a wide pH range.²¹⁻²⁵

59 In this work, we used silica coated quantum dots (QD@SiO₂) as a model nanoparticle system
60 to investigate zwitterionic ligands, and compare them to PEG ligands, with respect to colloidal
61 stability and cellular uptake. Semiconductor quantum dots (QDs) are attractive candidates as
62 luminescent probes for cell labeling and bioimaging. For optimal properties, colloidal QDs are
63 best synthesized in non-polar solvents, stabilized with hydrophobic ligands. Bio-applications of
64 QDs therefore typically involve a transfer to aqueous media. To this end, the encapsulation of QDs
65 in silica nanoparticles has been widely adopted in the past, and the reverse microemulsion
66 approach is an efficient method to make these QD@SiO₂ nano-objects.^{26, 27} During the
67 encapsulation process, the organic ligands on the surface of the QDs are substituted for hydrolyzed
68 silica monomers resulting in a tight interaction between the QD and the silica matrix.²⁸ Recently
69 developed core-shell CdSe/CdS QDs have shown superior optical properties with particularly
70 robust emission when encapsulated in silica, even in oxidative aqueous environments.²⁹ The silica
71 matrix additionally provides a convenient platform for the versatile surface functionalization of
72 these NPs with a large variety of organosilanes.

73 Based on this system, here we report the surface functionalization of QD@SiO₂ NPs with either
74 zwitterionic sulfobetaine-silane (SBS) or PEG-silane, followed by in-depth characterization via an
75 extensive Nuclear Magnetic Resonance (NMR) toolbox.³⁰ Particular attention was given to the
76 ligand density, which was determined by quantitative ERETIC (Electronic REference To access
77 In vivo Concentrations) method. The colloidal stability of these NPs was evaluated in water and
78 in crowded cell culture medium, demonstrating excellent colloidal stability for both ligand
79 systems. Cellular uptake in HeLa cells incubated with NPs was then investigated by confocal
80 fluorescence microscopy and flow cytometry. We demonstrate that, while even low ligand
81 densities of PEG considerably inhibit cellular uptake of the NPs, for zwitterionic functionalized
82 NPs there is an optimal window of ligand density in which good colloidal stability concurs with
83 efficient endocytosis. Finally, cytotoxicity assays showed no adverse effects of these NPs,
84 highlighting the strong potential of zwitterionic functionalized inorganic NPs for intracellular
85 applications.

86
87

88 2. Experimental Section

89

90 **2.1. Materials.** CdO (≥99.99%), oleyl alcohol (OIOH, 85%), BrijL4 (average Mn~362 g/mol),
91 tetraethyl orthosilicate (99.999%), 1,3-propane sultone (98%) and deuterated water (D₂O, 99.9%)
92 were purchased from Sigma-Aldrich. n-Tetradecylphosphonic acid (TDPA, ≥97%) was purchased

93 from PlasmaChem GmbH. Trioctylphosphine (TOP, $\geq 97\%$) and sulfur (S, 99.999%) were
94 purchased from Strem Chemicals. Trioctylphosphine oxide (TOPO, $\geq 98\%$), dimethyl sulfoxide
95 and deuterated dimethyl sulfoxide (DMSO d^6 , 99.8%) were purchased from Merck Millipore.
96 Selenium powder (Se, 200 mesh, 99.999%) and oleic acid (OA, 90%) were purchased from Alfa
97 Aesar. n-Heptane and ammonia solution (32%) were purchased from VWR Chemicals. 3-
98 [Methoxy(polyethyleneoxy)propyl]trimethoxysilane (PEG-silane, 90%, 9-12 PE-units) and (N,N-
99 dimethyl-3-aminopropyl)trimethoxysilane (97%) were purchased from abcr. Toluene and
100 methanol were purchased from Fiers. The HeLa cell culture medium is composed of DMEM/F12
101 medium (Gibco) with penicillin/streptomycin (Gibco), L-glutamine (Gibco) and supplemented
102 with 10% Fetal Bovine Serum (FBS). All cell culture products were purchased from Life
103 Technology unless specifically stated.

104 **2.2. Synthesis of the CdSe/CdS QDs.** The CdSe/CdS core-shell QDs used in this study
105 consisted of a 3.3 nm wurtzite CdSe core with a 2.1 nm thick CdS shell for a total diameter of 7.5
106 nm. They were synthesized according to the *flash* procedure reported in the literature.^{31,32} The full
107 synthesis details are given in the Supporting Information.

108 **2.3. Synthesis of 3-(dimethyl(3-(trimethoxysilyl)propyl)ammonio)propane-1-sulfonate.**
109 The synthesis of the zwitterionic sulfobetaine-silane (SBS), was adapted from a method reported
110 in the literature.¹⁸ In a glovebox under nitrogen, 0.2 mL (2.23 mmol) of 1,3-propane sultone was
111 dissolved in 3 mL of dimethyl sulfoxide (DMSO). Then, 0.5 mL (2.20 mmol) of (N,N-dimethyl-
112 3-aminopropyl)trimethoxysilane was added and the reaction mixture was allowed to stir for 24
113 hours. The solution was stored under inert atmosphere and used as is. The SBS concentration was
114 found to be about 0.55 M as determined by quantitative NMR analyses (see Results section).

115 **2.4. Silica encapsulation and surface functionalization.** The CdSe/CdS QDs were
116 encapsulated in silica through a reverse microemulsion process according to a procedure described
117 in the literature.²⁹ In a round-bottom flask, 10 nmol of QDs were dispersed in a mixture of 50 mL
118 of heptane and 16 mL of Brij L4 surfactant. After 5 minutes under stirring, 2.5 mL of a 5 %
119 ammonia solution in water was added to the mixture. After 1 h under stirring, 100 μ L of tetraethyl
120 orthosilicate (TEOS) was added to the mixture and allowed to stir for 3 days. For bare QD@SiO₂
121 NPs, the reaction was stopped at this point by adding 25 mL of ethanol to destabilize the
122 microemulsion. The NPs were then collected by centrifugation (5000 g, 10 min) and washed once
123 with ethanol and twice with water. The NPs were then dispersed and stored in 3 mL of water. For
124 SBS or PEG functionalized QD@SiO₂ NPs, the corresponding silane precursor was added directly
125 to the microemulsion and the reaction was allowed to stir for another 2 days. The reaction was
126 then stopped by adding 25 mL of ethanol and the NPs were collected by centrifugation (5000 g,
127 10 min). The NPs were first washed with ethanol. While SBS functionalized NPs were not stable
128 in ethanol and could easily be collected by centrifugation (5000 g, 10 min), PEG functionalized
129 NPs were too stable to be collected by centrifugation. In this case, the NPs were collected by using
130 spin filters (VivaSpin, 100 kDa MWCO) and centrifugation (2200 g, 20 min). The NPs were then
131 washed three times in water, in which case both SBS and PEG functionalized NPs are very stable
132 and therefore collected with spin filters and centrifugation (2200 g, 20 min). Finally, the NPs were
133 dispersed and stored in 3 mL of water.

134 **2.5. Material Characterization.** Transmission electron microscopy (TEM) images were
135 acquired using a Cs-corrected JEOL 2200FS microscope operating at 200 kV. UV-vis absorption
136 spectra were acquired using a PerkinElmer Lambda 950 spectrometer. Dynamic light scattering
137 (DLS) and zeta potential measurements were performed using a Malvern Zetasizer Nano Series.
138 For these measurements, the NPs were diluted 200 times in either double distilled water or cell

139 culture medium. The DLS determined hydrodynamic diameters are expressed as Z-averages. For
140 nuclear magnetic resonance (NMR) measurements, about 10 nmol of QD@SiO₂ NPs in water was
141 spin filtered and redispersed with 1 ml of D₂O. The sample was then upconcentrated to about 200
142 μl by spin filtration, transferred to a 5 mm NMR tube and the volume was adjusted to 500 μL with
143 D₂O. The NMR data were collected on a Bruker Avance II spectrometer operating at a ¹H
144 frequency of 500.13 MHz and equipped with a PATXO probe (¹H, ¹³C and ¹⁹F). Quantitative ¹H
145 spectra were acquired by using the Digital ERETIC method with a 20 s delay between scans to
146 allow for full relaxation. The ¹H-¹H correlation spectroscopy (COSY), the ¹H-¹³C heteronuclear
147 single quantum correlation spectroscopy (HSQC) and the ¹H-¹³C heteronuclear multiple bond
148 correlation spectroscopy (HMBC) spectra were acquired using standard pulse sequences from the
149 Bruker library, cosygpppqf, hsqcedtgsisp and hmbcgpplndqf, respectively. The delay was set to
150 long-range ⁿJ¹H¹³C coupling of 8 Hz in the ¹H-¹³C HMBC, while the one bond ¹J¹H¹³C coupling
151 correlations were filtered out. All three heteronuclear correlations were processed in magnitude
152 mode using a sine bell window function. The 2D diffusion correlated spectroscopy (DOSY) was
153 performed using a double-stimulated echo sequence for convection compensation and with bipolar
154 gradient pulses.³³ Smoothed rectangle gradient pulse shapes were used throughout. The gradient
155 strength was varied linearly from 2 to 95% of the probe's maximum value (calibrated at 50.1 G/cm)
156 in 64 steps, with the gradient pulse duration and diffusion delay optimized to ensure a final
157 attenuation of the signal in the final increment of less than 10% relative to the first increment. The
158 diffusion coefficients were obtained by fitting the appropriate Stejskal-Tanner (Equation 1) to the
159 signal intensity decay,³⁴ where I₀ is the initial signal intensity, D is the diffusion coefficient (m²/s),
160 γ is gyromagnetic ratio (MHz/T), g is the gradient strength (T/m), δ is the gradient pulse duration
161 (s) and Δ is the diffusion delay (s).

$$I = I_0 e^{-D\gamma^2 g^2 \delta^2 (\Delta - 0.6\delta)} \quad \text{Equation 1}$$

162
163
164
165 **2.6. Cell culture, fluorescence confocal microscopy and toxicity assay.** HeLa cells (ATCC®
166 CCL-2™) were cultured in DMEM/F-12 (Gibco-Invitrogen) supplemented with 10% heat-
167 inactivated fetal bovine serum (FBS, Biowest), 2 mM glutamine (Gibco-Invitrogen), and 100
168 U/mL penicillin/streptomycin (Gibco-Invitrogen). Cells were passaged using DPBS (Gibco-
169 Invitrogen) and trypsin-EDTA (0.25%, Gibco-Invitrogen). HeLa cells were cultivated in a
170 humidified tissue culture incubator at 37 °C and 5% CO₂. For confocal microscopy, 15000 HeLa
171 cells were seeded per well in a 96-well plate one day in advance. The NPs were diluted in cell
172 culture medium to a concentration of 30 nM, and 200 μL of the suspended solution was added into
173 each well. After 4 hours of incubation at 37 °C, the solution was discarded and the cells were
174 washed twice with DPBS. Fluorescence confocal microscopy imaging was performed on a
175 spinning disk confocal microscope (Nikon eclipse Ti-e inverted microscope, Nikon) equipped with
176 an MLC 400 B laser box (Agilent technologies), a Yokogawa CSU-22 Spinning Disk scanner
177 (Andor) and an iXon ultra EMCCD camera (Andor Technology, Belfast, UK) with a 60× oil
178 immersion objective (CFI Plan Apo VC, Nikon). A 405 nm laser was used as excitation and the
179 emission was recorded in the 640 nm channel. For the flow cytometry measurements, the same
180 incubation procedure was performed. The HeLa cells were then detached by trypsin-EDTA
181 treatment and collected by centrifugation. After the cells were re-suspended in flow buffer (DPBS
182 supplemented with 1% Bovine Serum Albumin (BSA) and 0.1% NaN₃), the samples were
183 measured by flow cytometry (Cytoflex, Beckman Coulter). 8000 cells were set to be measured for
184 one sample. A 408 nm laser was used as excitation and the emission was recorded in the 610/20

185 nm channel. Positive cells were defined when the fluorescence signals were higher than for the
186 control group. Cytotoxicity was measured by the *CellTiter Glo* assay. After 4 hours of incubation
187 with the NPs, the cells were washed twice with DPBS. Afterwards, 100 μ L of fresh cell culture
188 medium and 100 μ L of *CellTiter Glo* solution (CellTiter-Glo[®] Luminescent Cell Viability Assay,
189 Promega) were added into each well. The mixture was then allowed to shake for 10 min at 100
190 rpm, and the luminescence was measured by GloMax (GloMax[®] 96 Microplate Luminometer,
191 Promega).

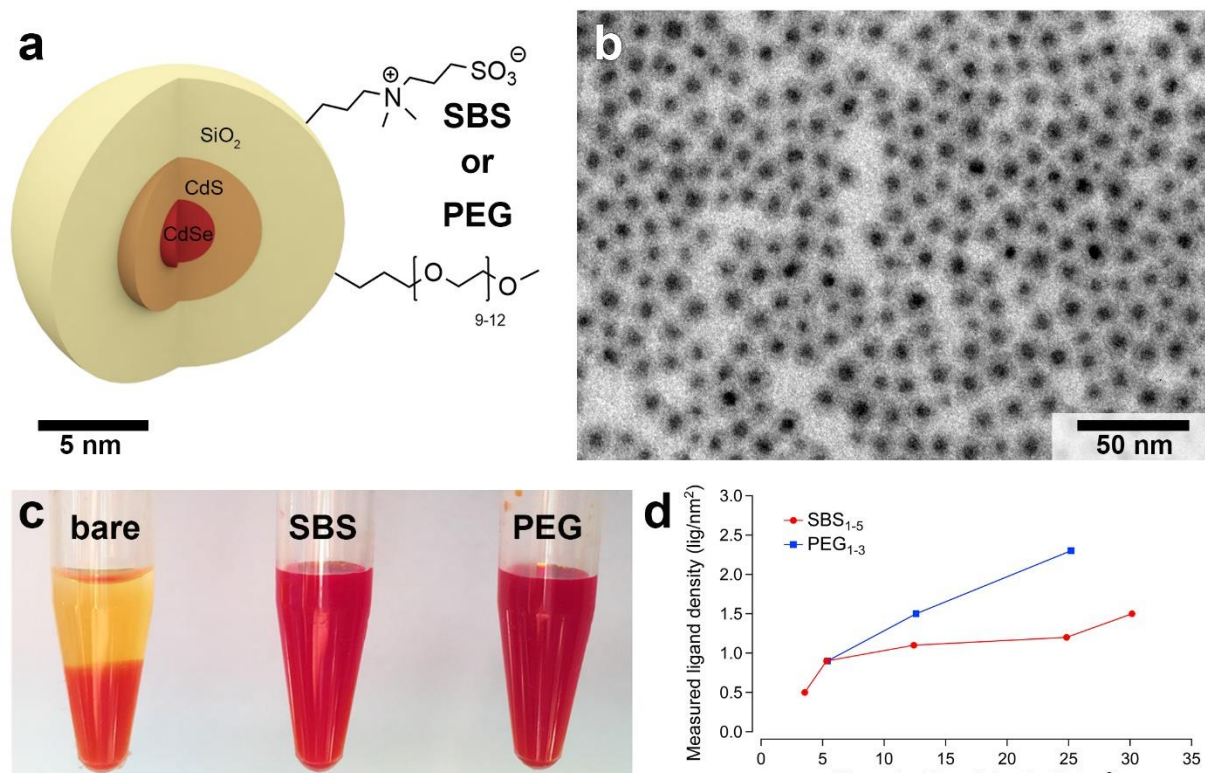
192
193

194 **3. Results and Discussion.**

195

196 **3.1. SBS and PEG functionalized QD@SiO₂ NPs.** In contrast to PEG-silane which is well
197 documented and commercially available, SBS was synthesized in-house through a modified
198 procedure from literature.¹⁸ In this work, SBS was synthesized in DMSO instead of acetone. Since
199 SBS is not soluble in acetone, the original synthesis method involved precipitation with subsequent
200 purification steps, and the product was stored and used as a dry powder. In our experience, this
201 resulted in a rather short shelf life, typically less than two weeks, for SBS which is easily prone to
202 hydrolysis. Thanks to our modified synthesis method, the SBS, which is soluble in DMSO, could
203 be used as is, directly from the synthesis solution without the need of additional purification steps,
204 with shelf life up to several months. The SBS chemical structure was confirmed by ¹H NMR, as
205 well as DOSY, COSY, HSQC and HMBC measurements (Figure 1 and Supporting Information,
206 Figure S1). In Figure 1a, all the resonances with a significant intensity can be assigned to SBS (see
207 the Supporting Information, Figure S1, for the detailed structure analysis). A diffusion coefficient
208 of 205 μ m²/s was determined by DOSY analysis of the as-synthesized SBS, which is the expected
209 value for a \sim 1 nm molecule that diffuses freely in solution (Figure 1b). Integrating the whole set
210 of resonances between 0.5 ppm and 3.7 ppm in the DOSY measurements resulted in a mono-
211 exponential intensity drop with increasing square field gradient strength, indicating that no shorter
212 molecules, e.g. unreacted precursors or impurities, are present in significant amounts. The analysis
213 of the as-synthesized product by quantitative ERETIC indicated a SBS concentration of 0.55 M
214 (signals integrated from 0.52 to 0.8 ppm). When compared to the theoretical concentration that
215 could have been achieved with a full conversion of the (N,N-dimethyl-3-
216 aminopropyl)trimethoxysilane, this concentration corresponds to a chemical yield of 93%,
217 consistent with the 90% yield reported with the original method.¹⁸ These observations and the high
218 chemical yield of the synthesis justified using this synthesized product without further purification.

219



236
 237 **Figure 2. a**, Illustration of a QD@SiO₂ NP with either SBS or PEG surface functionalization. **b**, TEM image of SBS
 238 functionalized NPs. **c**, Photograph of bare, SBS and PEG functionalized QD@SiO₂ NPs in water. **d**, Experimentally
 239 determined ligand density as a function of theoretical amount added to the synthesis.
 240

241 The TEM image in Figure 2b shows that each QD is encapsulated in a silica shell (see the
 242 Supporting Information, Figure S2, for additional TEM images). This constitutes a great asset for
 243 the quantitative analysis of the particle surface chemistry. In combination with the intrinsic
 244 absorption coefficient of the QDs, it enables determination of the concentration of NPs in a
 245 dispersion by means of a single UV-vis absorption measurement.^{36, 37} Indeed, UV-vis absorption
 246 spectra of SBS and PEG functionalized NPs in water overlap quite well with that of the QDs
 247 measured in toluene (Supporting Information, Figure S3). Results suggest that the QD absorption
 248 spectrum is not significantly affected by light scattering, corroborating good colloidal stability.
 249 Figure 1a compares the ¹H NMR spectra of SBS functionalized NPs in D₂O and free SBS (see the
 250 Supporting Information, Figure S4, for the same analysis on PEG functionalized NPs, and Figure
 251 S5 for the DOSY analysis of all samples). As expected for organic ligands bound to the surface of
 252 larger NPs, the NMR signals of the SBS protons show strongly broadened features (Figure 1a),
 253 due to their slower tumbling rate in solution.³⁰ The signals of protons #2 and #3, which are the
 254 closest to the NPs, are subject to substantial broadening and therefore not observable in the NMR
 255 spectrum of the bound SBS. Protons from the methoxy groups have disappeared due to the
 256 hydrolysis and binding of SBS to the surface. While the signals of protons #4, #5, #6 and #8
 257 correspond to the more intense signals from 2.75 ppm to 3.75 ppm, the signal of proton #7 is
 258 isolated at 2.25 ppm and is ideal to integrate for quantitative spectra analysis. In combination with
 259 the known NP concentration and size, the ligand density could be determined by integrating this
 260 bound resonance in a quantitative ¹H NMR spectrum. It should be noted that such a quantification

disregards any deviation from a spherical surface, for example, due to porosity of the SiO₂ shell, such that a nominal rather than an actual ligand density is obtained.

In this work, NPs with varying ligand densities were synthesized by adding different amounts of SBS or PEG-silane to the synthesis. Table 1 summarizes characterization results for the different samples investigated, namely SBS₁₋₅ and PEG₁₋₃, with the respective measured ligand densities and other parameters (diameter, hydrodynamic diameter, zeta potential, positive cell percentage). Figure 2d shows the relation between the theoretical amount of ligand added to the reaction mixture and the experimentally measured value. The trends indicate that a significant excess of the ligand-silane is needed to achieve sufficient surface coverage. The surface of SBS functionalized NPs seems to saturate at about 1.5 lig/nm², whereas ligand density for PEG functionalized NPs kept increasing with increasing the amount of precursor. SBS functionalized NPs with ligand density from 0.5 to 1.5 lig/nm², and PEG functionalized NPs with ligand densities from 0.9 to 2.3 lig/nm² were thus investigated and compared to bare NPs. One should note that further reducing the ligand density below 0.9 lig/nm² typically resulted in NPs with poor colloidal stability, as observed from visible aggregation during the purification procedure. The surface functionalization of the QD@SiO₂ NPs had a limited impact on their zeta potential (Table 1). As expected, the bare NPs have a negative zeta potential of -27.2 mV due to the deprotonation of silanol groups in water.³⁸ For SBS functionalized NPs, the zeta potential decreases continuously with increasing the ligand density, down to -16.7 mV for the highest density, which could be explained by partial charge screening and reduction of surface silanol groups due to the binding of ligands. On the other hand, for PEG functionalized NPs, the zeta potential decreased to about -19.5 mV, regardless of the ligand density.

Table 1. Summary of characterization results for samples investigated in this study providing ligand density, average diameter measured by TEM, hydrodynamic diameters measured by DOSY and DLS, zeta potential and resulting positive cell percentage (PCP) after incubation with HeLa cells at 30 nM for 4 hours.

sample	ligand density (lig/nm ²) ^a	TEM (nm) ^b	DOSY (nm) ^c	DLS (nm) ^d	zeta potential (mV) ^d	PCP (%) ^d
bare	-	14.6 ± 0.9	-	597 ± 120	-27.2 ± 2.1	94.7 ± 1.7
SBS ₁	0.5 ± 0.1	14.4 ± 1.1	49.5 ± 4.6	77.7 ± 2.5	-22.4 ± 0.7	99.9 ± 1.0
SBS ₂	0.9 ± 0.1	15.0 ± 1.1	20.5 ± 0.5	21.5 ± 0.8	-20.7 ± 2.9	97.3 ± 1.0
SBS ₃	1.1 ± 0.1	13.7 ± 1.1	23.1 ± 1.1	22.3 ± 3.6	-17.5 ± 1.7	47.2 ± 7.9
SBS ₄	1.2 ± 0.1	14.5 ± 1.2	19.2 ± 1.7	23.2 ± 1.4	-16.6 ± 1.2	15.4 ± 0.2
SBS ₅	1.5 ± 0.2	14.7 ± 1.1	21.1 ± 0.7	21.4 ± 6.1	-16.7 ± 0.7	1.5 ± 0.3
PEG ₁	0.9 ± 0.1	15.1 ± 1.1	21.4 ± 0.2	20.6 ± 1.2	-19.3 ± 0.9	2.7 ± 0.1
PEG ₂	1.5 ± 0.2	15.2 ± 1.0	23.3 ± 0.3	21.0 ± 0.5	-19.5 ± 1.9	2.5 ± 0.1
PEG ₃	2.3 ± 0.2	14.8 ± 1.1	20.0 ± 0.6	23.8 ± 0.9	-19.5 ± 0.6	1.6 ± 0.2

^a error determined by propagating the integration error of the ERETIC NMR signal in the ligand density calculation.

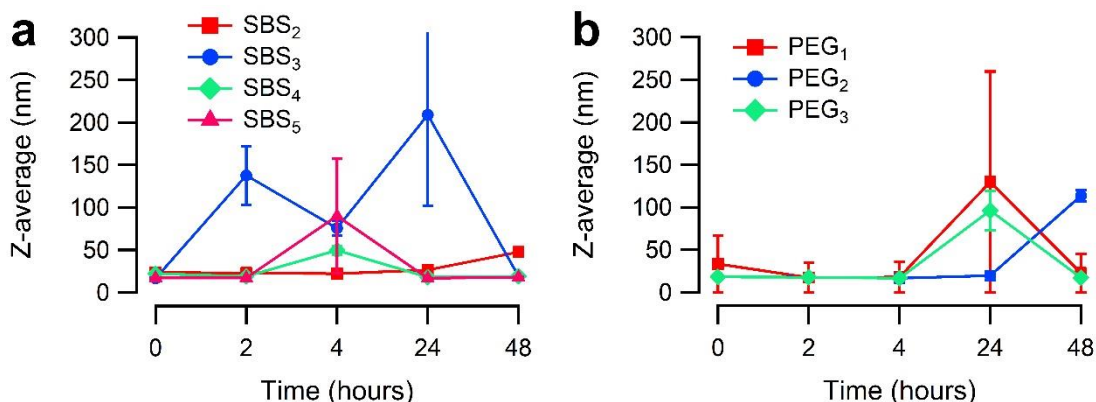
^b average value and standard deviation based on the sizing of over 200 NPs.

^c error determined by propagating the error on the mono-exponential fitting in the diffusion coefficient calculation.

^d average value and standard deviation from three replicate experiments.

3.2. Colloidal stability of SBS and PEG functionalized QD@SiO₂ NPs. The colloidal stability of these NPs was first examined in water, through a measurement of their hydrodynamic diameter by DLS and DOSY (Table 1 and Supporting Information, Figure S5). As already evidenced by visual observation (Figure 2c), the bare QD@SiO₂ NPs show substantial sedimentation, highlighting the need for surface functionalization to ensure colloidal stability. The aggregation of bare NPs can also be seen in their UV-vis absorption spectrum, which shows typical

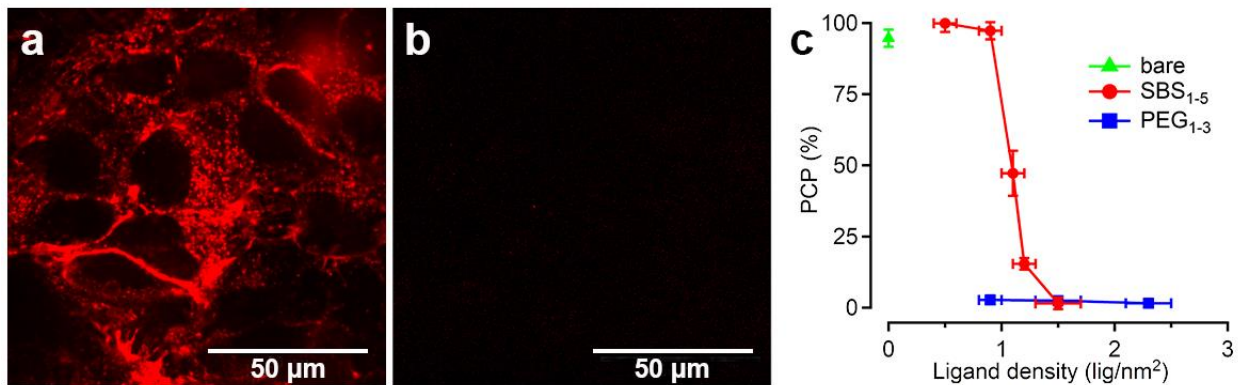
299 light scattering features (Supporting Information, Figure S3). Although bare NPs could not be
 300 measured by DOSY, the DLS measurement resulted in a very large Z-average value of about 600
 301 nm, in line with the formation of sizeable aggregates. Similarly, the SBS functionalized NPs with
 302 the lowest ligand density (SBS₁) showed hydrodynamic diameters of 49.5 nm and 77.7 nm, as
 303 measured by DOSY and DLS, respectively. These values cannot be attributed to individual NPs,
 304 indicating a limited but existing degree of aggregation in this case as well. All other SBS and PEG
 305 functionalized samples show hydrodynamic diameters in the range of 20 to 23 nm for both DLS
 306 and DOSY measurements. These values are consistent with the NP diameter as measured by TEM,
 307 plus the ligand and solvation shells, indicating that these samples are free of aggregation. Their
 308 colloidal stability was further assessed by DLS measurements in the cell culture medium to
 309 determine longer term stability in a crowded biological environment (Figure 3). Despite some
 310 fluctuations, the Z-average values do not show any continuous and persistent increase during the
 311 48 hours experiment duration, indicating that both SBS and PEG functionalized NPs remained
 312 stable. These results confirm the equivalent efficiency of these two ligand systems to preserve
 313 colloidal stability during the cell incubation step, which typically only last for a few hours.
 314



315
 316 **Figure 3.** DLS measurements on SBS functionalized QD@SiO₂ NPs (a) and PEG functionalized QD@SiO₂ NPs (b)
 317 in cell culture medium over a 48 hours period.
 318

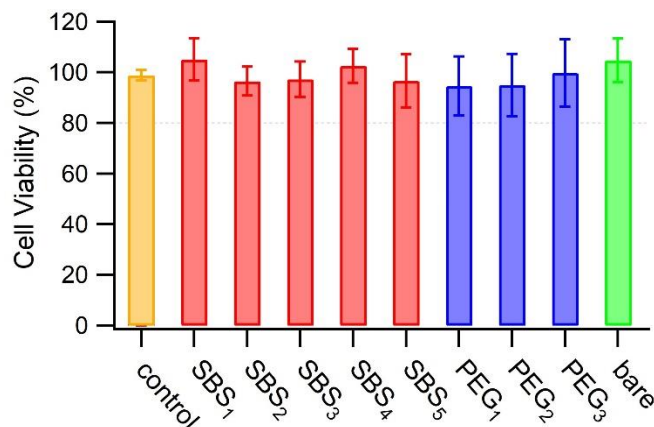
319 **3.3. Cellular uptake and toxicity assay.** Thanks to the luminescence property of the QDs, the
 320 cellular uptake of NPs could be investigated by fluorescence confocal microscopy imaging (Figure
 321 4a-b and Supporting Information, Figure S6). As previously demonstrated, the optical properties
 322 of such *flash* grown QDs are preserved after silica coating.²⁹ The confocal images reveal that at
 323 similar ligand densities, SBS functionalized NPs show a high degree of uptake with a lot of
 324 luminescence coming from the cells, whereas with PEG functionalized NPs the cells hardly show
 325 any detectable uptake. In addition, bare QD@SiO₂ NPs also show a high degree of endosomal
 326 uptake (Supporting Information, Figure S6i), corroborating our previous study on such
 327 unfunctionalized NPs.²⁹ The propensity for cellular uptake was then carefully quantified by flow
 328 cytometry measurements to determine the positive cell percentage (PCP, Figure 4c and Table 1).
 329 In line with the observation from the fluorescence confocal images, the cells show very high levels
 330 of NP uptake with the PCP approaching 100% in the case of bare NPs and SBS functionalized NPs
 331 with low ligand densities. The uptake then decreases drastically with increasing SBS ligand
 332 density, with nearly no uptake for the NPs with the highest ligand density. Flow cytometry
 333 measurements confirmed the very low uptake of PEG functionalized NPs regardless of the ligand
 334 density. Since the molecular weight of the PEG ligands is more than twice the molecular weight

335 of the SBS ligands, the PCP are also represented as a function of ligand mass density in the
 336 Supporting Information, Figure S7, highlighting the difference in nature of these two ligand
 337 systems. However, NPs with PEG falling in the range of ligand mass densities for which high
 338 cellular uptake was achieved with zwitterionic ligands, were not stable enough to be investigated.
 339



340 **Figure 4.** Fluorescence confocal microscopy images of HeLa cells incubated with SBS functionalized QD@SiO₂ NPs
 341 (a, sample SBS₂) and PEG functionalized QD@SiO₂ NPs (b, sample PEG₁). c, Positive cell percentage (PCP) as a
 342 function of the ligand type and ligand density.
 343
 344

345 In parallel to cellular uptake measurements, cell viability was assessed by *CellTiter Glo*
 346 luminescent assay (Figure 5). The results show no significant effect on the HeLa cells, with cell
 347 viability well above 80% at the investigated concentration, regardless of the surface chemistry of
 348 the QD@SiO₂ NPs. Thus, even at high levels of endocytosis, the NPs remain benign for the cells,
 349 making them relevant for intracellular bio-applications.
 350



351 **Figure 5.** Viability of HeLa cells after incubation (4 hours, 30 nM) with SBS (red) and PEG (blue) functionalized NPs
 352 as well as bare NPs (green), determined by *CellTiter Glo* luminescent cell viability assay. For the control experiment
 353 (yellow), the cells underwent the same process, except that no NPs were added.
 354
 355

356 **3.4. Discussion.** While bare NPs offer high uptake levels as previously reported,²⁹ they suffer
 357 from unsatisfying colloidal properties with substantial levels of aggregation. Since the properties
 358 of inorganic nanoparticles often arise from their reduced dimension itself, this effect strongly
 359 impairs their use for cell labeling and other biological applications. In addition, large objects with
 360 dimensions exceeding those of typical biomolecules could interfere negatively with the biological

361 process or organelle being probed,³⁵ hence defeating the purpose of the analysis. In this work, we
362 show that this issue can be solved through the surface functionalization of NPs with either PEG or
363 zwitterionic SBS ligands. In line with previous reports,¹²⁻¹⁴ we observed that surface
364 functionalization with PEG ligands strongly inhibits their spontaneous uptake by live cells. In our
365 system and for our set of experimental conditions, we could not find a ligand density for PEG that
366 would provide sufficient colloidal stability while promoting cellular uptake. Indeed, further
367 reducing the ligand density from the value reported for PEG₁ sample (0.9 lig/nm²) resulted in
368 apparent aggregation of the NPs. On the other hand, efficient uptake of SBS functionalized NPs
369 was observed, which at first seems contradictory to previous literature reports on the inhibiting
370 effect of zwitterionic ligands on cellular uptake.^{20, 23} However, these studies did not report a
371 detailed investigation of the effects of ligand density. Our work confirms that for high SBS ligand
372 densities, the ligands quantitatively inhibit cellular uptake. In contrast, a sweet spot exists at lower
373 ligand densities, where efficient uptake can be achieved without compromising colloidal stability.
374 For example, sample SBS₂ (0.9 lig/nm²) showed the highest level of uptake (Figure 4a and c) while
375 offering fully satisfying colloidal stability (Figure 3). Lowering the ligand density to 0.5 lig/nm²
376 (sample SBS₁) hardly increases the positive cell percentage (Figure 4c), while inducing some
377 aggregation (Table 1), thus not meeting the quality criteria expected for these materials. The effect
378 of the ligand shell on the zeta potential of these NPs alone cannot explain these differences in
379 uptake propensity since SBS functionalized NPs with lower zeta potentials (samples SBS₃₋₄) than
380 the PEG functionalized NPs still showed higher uptakes. Although the effect of sedimentation on
381 the uptake of bare NPs could be considered,¹³ the data on SBS functionalized NPs with optimal
382 colloidal stability and uptake levels similar to those of bare ones indicate, that this is not the main
383 mechanism at play here. Taken together, these results suggest that at low ligand density, the surface
384 exposed by SBS functionalized NPs still resembles enough the bare silica surface to undergo the
385 same internalization process, which was demonstrated to follow an endocytic pathway,²⁹ while
386 providing sufficient steric stabilization to prevent the NPs from aggregating. The incomplete
387 coverage of the nanoparticle surface and remaining exposed charges can lead to the adsorption of
388 proteins present in the culture medium supplemented with serum, which can play a role in the
389 cellular uptake of zwitterionic functionalized nanoparticles with low ligand density.^{39, 40} The use
390 of zwitterionic ligands hence shows to be an extremely promising route in order to purposefully
391 control the interaction between NPs and cells, with important potential for specific targeting and
392 controlled release strategies.⁴¹ Tuning the ligand density of these NPs offers a practical knob to
393 balance their ‘stealth’ character (circulation, non-specific binding), which is achieved at high
394 ligand density, whereas their non-targeted cell internalization is promoted at the other end of the
395 spectrum by a low ligand density.

396

397

398 **4. Conclusion.**

399

400 Using luminescent CdSe/CdS@SiO₂ NPs of about 15 nm diameter as a model system, we
401 optimized the surface chemistry of these NPs in order to balance colloidal stability and cellular
402 uptake. Commonly used PEG ligands were compared to sulfobetaine zwitterionic ligands,
403 highlighting the superiority of the latter in promoting spontaneous uptake by live cells. Through a
404 careful quantitative analysis of the ligand density by NMR spectroscopy, we identified an optimal
405 window for the surface functionalization of these NPs with zwitterionic ligands. NPs with SBS
406 ligand densities at around 1 lig/nm² show an ideal combination of good colloidal stability in

407 crowded cell medium and efficient spontaneous cellular uptake. At lower ligand densities, the NPs
408 aggregate, and at higher densities, uptake is inhibited. The zwitterionic functionalization of NPs
409 therefore offers an alternative strategy for the design of intracellular probes without the need to
410 implement costly targeting ligands. We believe that this approach can be extended to other
411 inorganic NPs with a wide range of properties and compositions, therefore enabling a number of
412 intracellular applications based on these materials.

413
414

415 **Acknowledgments**

416 This project has received funding from the European Union's Horizon 2020 research and
417 innovation programme under the Marie Skłodowska-Curie grant agreements No 702300, No
418 642656, and No 691185 (H2020-MSCA-ITN-642656, MSCA-IF-2015-702300 and MSCA-RISE-
419 691185). The authors acknowledge BelSPo (IAP 7.35, photonics@be), FWO-Vlaanderen (KaN
420 1509012N), Ghent University (GOA/01G01513; BOF14/PDO/007; IOP/01IO1214), and IWT-
421 Vlaanderen for financial support. The 500 MHz equipment used in this work was funded through
422 a grant from the Hercules foundation (AUGE09/006). K. B. acknowledges financial support by
423 the European Research Council (ERC) under the European Union's Horizon 2020 research and
424 innovation program (grant agreement No 648124). J. L. gratefully acknowledges the financial
425 support from the China Scholarship Council (CSC) (201506750012) and the Special Research
426 Fund from Ghent University (01SC1416).

427
428

428 **Associated content**

429 The Supporting Information is available free of charge via the Internet.
430 Synthesis details of the QDs, optical characterization, additional NMR analyses, TEM images,
431 DLS measurements, and fluorescence confocal images.

432
433

433 **Notes**

434 The authors declare no competing financial interest.

435
436

437 **References**

438

- 439 1. Zhang, L.; Gu, F. X.; Chan, J. M.; Wang, A. Z.; Langer, R. S.; Farokhzad, O. C., Nanoparticles
440 in Medicine: Therapeutic Applications and Developments. *Clin. Pharmacol. Ther.* **2008**, 83, (5),
441 761-769.
- 442 2. Wang, M.; Thanou, M., Targeting nanoparticles to cancer. *Pharmacol. Res.* **2010**, 62, (2), 90-
443 99.
- 444 3. Riehemann, K.; Schneider, S. W.; Luger, T. A.; Godin, B.; Ferrari, M.; Fuchs, H.,
445 Nanomedicine—Challenge and Perspectives. *Angew. Chem. Int. Ed.* **2009**, 48, (5), 872-897.
- 446 4. Mout, R.; Moyano, D. F.; Rana, S.; Rotello, V. M., Surface functionalization of nanoparticles
447 for nanomedicine. *Chem. Soc. Rev.* **2012**, 41, (7), 2539-2544.
- 448 5. Chou, L. Y. T.; Ming, K.; Chan, W. C. W., Strategies for the intracellular delivery of
449 nanoparticles. *Chem. Soc. Rev.* **2011**, 40, (1), 233-245.
- 450 6. Phillips, E.; Penate-Medina, O.; Zanzonico, P. B.; Carvajal, R. D.; Mohan, P.; Ye, Y.; Humm,
451 J.; Gönen, M.; Kalaigian, H.; Schöder, H.; Strauss, H. W.; Larson, S. M.; Wiesner, U.; Bradbury,

452 M. S., Clinical translation of an ultrasmall inorganic optical-PET imaging nanoparticle probe. *Sci.*
453 *Transl. Med.* **2014**, 6, (260), 260ra149.

454 7. Yameen, B.; Choi, W. I.; Vilos, C.; Swami, A.; Shi, J.; Farokhzad, O. C., Insight into
455 nanoparticle cellular uptake and intracellular targeting. *J. Control. Release* **2014**, 190, 485-499.

456 8. Leckband, D.; Sheth, S.; Halperin, A., Grafted poly(ethylene oxide) brushes as nonfouling
457 surface coatings. *J. Biomater. Sci. Polym. Ed.* **1999**, 10, (10), 1125-1147.

458 9. Thierry, B.; Zimmer, L.; McNiven, S.; Finnie, K.; Barbé, C.; Griesser, H. J., Electrostatic Self-
459 Assembly of PEG Copolymers onto Porous Silica Nanoparticles. *Langmuir* **2008**, 24, (15), 8143-
460 8150.

461 10. Ma, K.; Mendoza, C.; Hanson, M.; Werner-Zwanziger, U.; Zwanziger, J.; Wiesner, U.,
462 Control of ultrasmall sub-10 nm ligand-functionalized fluorescent core-shell silica nanoparticle
463 growth in water. *Chem. Mater.* **2015**, 27, (11), 4119-4133.

464 11. Ma, K.; Zhang, D.; Cong, Y.; Wiesner, U., Elucidating the Mechanism of Silica Nanoparticle
465 PEGylation Processes Using Fluorescence Correlation Spectroscopies. *Chem. Mater.* **2016**, 28,
466 (5), 1537-1545.

467 12. Pelaz, B.; del Pino, P.; Maffre, P.; Hartmann, R.; Gallego, M.; Rivera-Fernández, S.; de la
468 Fuente, J. M.; Nienhaus, G. U.; Parak, W. J., Surface Functionalization of Nanoparticles with
469 Polyethylene Glycol: Effects on Protein Adsorption and Cellular Uptake. *ACS Nano* **2015**, 9, (7),
470 6996-7008.

471 13. Cho, E. C.; Zhang, Q.; Xia, Y., The effect of sedimentation and diffusion on cellular uptake
472 of gold nanoparticles. *Nat. Nanotechnol.* **2011**, 6, 385-391.

473 14. Torrisi, V.; Graillot, A.; Vitorazi, L.; Crouzet, Q.; Marletta, G.; Loubat, C.; Berret, J. F.,
474 Preventing Corona Effects: Multiphosponic Acid Poly(ethylene glycol) Copolymers for Stable
475 Stealth Iron Oxide Nanoparticles. *Biomacromolecules* **2014**, 15, (8), 3171-3179.

476 15. García, K. P.; Zarschler, K.; Barbaro, L.; Barreto, J. A.; O'Malley, W.; Spiccia, L.; Stephan,
477 H.; Graham, B., Zwitterionic-Coated "Stealth" Nanoparticles for Biomedical Applications: Recent
478 Advances in Countering Biomolecular Corona Formation and Uptake by the Mononuclear
479 Phagocyte System. *Small* **2014**, 10, (13), 2516-2529.

480 16. Khung, Y. L.; Narducci, D., Surface modification strategies on mesoporous silica
481 nanoparticles for anti-biofouling zwitterionic film grafting. *Adv. Colloid. Interface. Sci.* **2015**, 226,
482 166-186.

483 17. Rouhana, L. L.; Jaber, J. A.; Schlenoff, J. B., Aggregation-Resistant Water-Soluble Gold
484 Nanoparticles. *Langmuir* **2007**, 23, (26), 12799-12801.

485 18. Estephan, Z. G.; Jaber, J. A.; Schlenoff, J. B., Zwitterion-Stabilized Silica Nanoparticles:
486 Toward Nonstick Nano. *Langmuir* **2010**, 26, (22), 16884-16889.

487 19. Schlenoff, J. B., Zwitteration: Coating Surfaces with Zwitterionic Functionality to Reduce
488 Nonspecific Adsorption. *Langmuir* **2014**, 30, (32), 9625-9636.

489 20. Ashraf, S.; Park, J.; Bichelberger, M. A.; Kantner, K.; Hartmann, R.; Maffre, P.; Said, A. H.;
490 Feliu, N.; Lee, J.; Lee, D.; Nienhaus, G. U.; Kim, S.; Parak, W. J., Zwitterionic surface coating of
491 quantum dots reduces protein adsorption and cellular uptake. *Nanoscale* **2016**, 8, (41), 17794-
492 17800.

493 21. Estephan, Z. G.; Schlenoff, P. S.; Schlenoff, J. B., Zwitteration As an Alternative to
494 PEGylation. *Langmuir* **2011**, 27, (11), 6794-6800.

495 22. Muro, E.; Pons, T.; Lequeux, N.; Fragola, A.; Sanson, N.; Lenkei, Z.; Dubertret, B., Small
496 and Stable Sulfobetaine Zwitterionic Quantum Dots for Functional Live-Cell Imaging. *J. Am.*
497 *Chem. Soc.* **2010**, 132, (13), 4556-4557.

498 23. Yang, W.; Ella-Menye, J.-R.; Bai, T.; Sinclair, A.; Jiang, S., Stable and Functionalizable
499 Quantum Dots with a Thin Zwitterionic Carboxybetaine Layer. *Langmuir* **2017**, 33, (35), 8784-
500 8789.

501 24. Breus, V. V.; Heyes, C. D.; Tron, K.; Nienhaus, G. U., Zwitterionic Biocompatible Quantum
502 Dots for Wide pH Stability and Weak Nonspecific Binding to Cells. *ACS Nano* **2009**, 3, (9), 2573-
503 2580.

504 25. Dembele, F.; Tasso, M.; Trapiella-Alfonso, L.; Xu, X.; Hanafi, M.; Lequeux, N.; Pons, T.,
505 Zwitterionic Silane Copolymer for Ultra-Stable and Bright Biomolecular Probes Based on
506 Fluorescent Quantum Dot Nanoclusters. *ACS Appl. Mater. Interfaces* **2017**, 9, (21), 18161-18169.

507 26. Selvan, S. T.; Tan, T. T.; Ying, J. Y., Robust, Non-Cytotoxic, Silica-Coated CdSe Quantum
508 Dots with Efficient Photoluminescence. *Adv. Mater.* **2005**, 17, (13), 1620-1625.

509 27. Darbandi, M.; Thomann, R.; Nann, T., Single Quantum Dots in Silica Spheres by
510 Microemulsion Synthesis. *Chem. Mater.* **2005**, 17, (23), 5720-5725.

511 28. Biermann, A.; Aubert, T.; Baumeister, P.; Drijvers, E.; Hens, Z.; Maultzsch, J., Interface
512 formation during silica encapsulation of colloidal CdSe/CdS quantum dots observed by in situ
513 Raman spectroscopy. *J. Chem. Phys.* **2017**, 146, (13), 134708.

514 29. Aubert, T.; Soenen, S. J.; Wassmuth, D.; Cirillo, M.; Van Deun, R.; Braeckmans, K.; Hens,
515 Z., Bright and Stable CdSe/CdS@SiO₂ Nanoparticles Suitable for Long-Term Cell Labeling. *ACS*
516 *Appl. Mater. Interfaces* **2014**, 6, (14), 11714-11723.

517 30. Hens, Z.; Martins, J. C., A Solution NMR Toolbox for Characterizing the Surface Chemistry
518 of Colloidal Nanocrystals. *Chem. Mater.* **2013**, 25, (8), 1211-1221.

519 31. Cirillo, M.; Aubert, T.; Gomes, R.; Van Deun, R.; Emplit, P.; Biermann, A.; Lange, H.;
520 Thomsen, C.; Brainis, E.; Hens, Z., “Flash” Synthesis of CdSe/CdS Core–Shell Quantum Dots.
521 *Chem. Mater.* **2014**, 26, (2), 1154-1160.

522 32. Drijvers, E.; De Roo, J.; Geiregat, P.; Fehér, K.; Hens, Z.; Aubert, T., Revisited Wurtzite
523 CdSe Synthesis: A Gateway for the Versatile Flash Synthesis of Multishell Quantum Dots and
524 Rods. *Chem. Mater.* **2016**, 28, (20), 7311-7323.

525 33. Connell, M. A.; Bowyer, P. J.; Adam Bone, P.; Davis, A. L.; Swanson, A. G.; Nilsson, M.;
526 Morris, G. A., Improving the accuracy of pulsed field gradient NMR diffusion experiments:
527 Correction for gradient non-uniformity. *Journal Magn. Reson.* **2009**, 198, (1), 121-131.

528 34. Sinnaeve, D., The Stejskal–Tanner equation generalized for any gradient shape—an
529 overview of most pulse sequences measuring free diffusion. *Concept. Magn. Reson. A* **2012**, 40A,
530 (2), 39-65.

531 35. Knopp, D.; Tang, D.; Niessner, R., Review: Bioanalytical Applications of Biomolecule-
532 Functionalized Nanometer-Sized Doped Silica Particles. *Anal. Chim. Acta* **2009**, 647, (1), 14-30.

533 36. De Geyter, B.; Hens, Z., The Absorption Coefficient of PbSe/CdSe Core/Shell Colloidal
534 Quantum Dots. *Appl. Phys. Lett.* **2010**, 97, (16), 161908.

535 37. Hens, Z.; Moreels, I., Light absorption by colloidal semiconductor quantum dots. *J. Mater.*
536 *Chem.* **2012**, 22, (21), 10406-10415.

537 38. Behrens, S. H.; Grier, D. G., The charge of glass and silica surfaces. *J. Chem. Phys.* **2001**,
538 115, (14), 6716-6721.

539 39. Ritz, S.; Schöttler, S.; Kotman, N.; Baier, G.; Musyanovych, A.; Kuharev, J.; Landfester, K.;
540 Schild, H.; Jahn, O.; Tenzer, S.; Mailänder, V., Protein Corona of Nanoparticles: Distinct Proteins
541 Regulate the Cellular Uptake. *Biomacromolecules* **2015**, 16, (4), 1311-1321.

